Available online at www.sciencedirect.com
SCIENCE DIRECT®
Journal of Sound and Vibration 273 (2004) 149–173
JOURNAL OF SOUND AND VIBRATION
www.elsevier.com/locate/jsvi

The steady state responses of s.d.o.f. viscous elasto-plastic oscillator under sinusoidal loadings

C.-S. Liu*, Z.-M. Huang

Department of Mechanical and Marine Engineering, Taiwan Ocean University, Keelung 202-24, Taiwan

Received 24 August 2001; accepted 16 April 2003

Abstract

Depending on the values of the parameters identified, the long-term behaviour of s.d.o.f. viscous elasto-plastic oscillator under sinusoidal loadings may be periodic with or without intermediate unloading, or elastic shakedown (including purely elastic). A new phase-plane estimation method for the steady state elasto-plastic solutions is presented. We identify three dimensionless ratios, namely damping ratio ζ, force ratio r_f and frequency ratio r_w, as well as an elastic-phase duration variable y. The new estimate offers closed-form formulae for the force ratio r_f and for the ductility ratio μ in terms of ζ, r_w and y. Applying numerical method to the function $r_f = r_f(\zeta, r_w, y)$, we can obtain the inverse function $y = y(\zeta, r_w, r_f)$, such that the variation of μ in terms of ζ, r_w and r_f can be evaluated. Alternatively, for a given ductility ratio, we can solve $\mu = \mu(\zeta, r_w, y)$ numerically for y and then obtain the curves of r_f versus r_w to meet specified ductility ratio. The proposed method can estimate the steady state responses for any applied load and forcing frequency. The results calculated are in very good agreement with the exact time-marching solutions. A simple criterion of parameters values for elastic shakedown is derived, by which we can calculate the maximum driving force amplitude to avoid structures oscillating in the plastic range. It is found that there exists a best driving force amplitude for maximizing dissipation efficiency. The distribution of periodic points with and without intermediate unloading in the parametric plane $(r_w, 1/r_f)$ for given damping ratio is clarified. The intermediate unloading motion region locates within the range of $r_w \leqslant \sqrt{1-\zeta^2}/3$, and its size decreases when damping ratio increases.

*Corresponding author. Tel.: +886-2-2462-2192; fax: +886-2-2462-0836.
E-mail address: csliu@mail.ntou.edu.tw (C.-S. Liu).

0022-460X/03/$ - see front matter © 2003 Elsevier Ltd. All rights reserved.
doi:10.1016/S0022-460X(03)00423-1

1. Introduction

Structures may respond linearly elastically under moderately small loading; however, when subjected to severe excitations, they would respond inelastically and exhibit hysteretic behaviour. Hysteretic models have been used for the inelastic design of structures. Recently, some kinds of non-linear hysteretic isolators have gotten a lot of applications due to their good hysteretic property to dissipate input energy. Both the analytical modelling and response prediction of hysteretic systems have been an area of ever-increasing interest.

The most commonly used model for describing the non-linear hysteretic restoring force–displacement behaviour is the bilinear elasto-plastic system [1–5], which includes perfectly elasto-plastic system [6–9] as a special case upon letting the post-yield stiffness be zero. For most of the proposed non-linear models, the differential equations of motion are used to analyze the responses of the modelled structures under external loadings. Those equations are usually solved by using step-by-step integration techniques to obtain the time histories of responses. However, for engineering purpose we may not specially concern the time histories of responses. Rather, it is the extreme values of the responses that convey crucial information about the system, which are closely related to the system behaviour in the steady state. Early, Caughey [1], according to the work of Kryloff and Bogoliuboff, has employed the slowly varying parameters method to present an analytic solution for the steady state response of the bilinear hysteretic oscillator to sinusoidal excitation. However, his estimation in the moderately low-frequency range is not accurate [10]. Since then more contributions to this vibration issue have been made; see, e.g., Capecchi and Vestroni [11,12], DebChaudhury [13], Badrakhan [14], Pratap and Holmes [15], and Reddy and Pratap [16]. Capecchi and Vestroni [11,12] have extended the same approach to study the steady-state response of more general yielding oscillators to harmonic excitation. DebChaudhury [13] has provided a piecewise linear approximation method, and Badrakhan [14] a polynomial approximation method to obtain steady state solution of the bilinear oscillator. Reddy and Pratap [16] proposed a variable equivalent viscous damping method for viscous bilinear oscillator. These methods should assume that either the steady state response is harmonic, or the response is not too large, or the bilinearity of the system does not deviate from the linearity too much. Furthermore, as pointed out by Miller and Butler [6] and Capecchi [8], the occurrence of intermediate unloading in steady state renders some of the above approximate methods unable to model.

In this paper a more concise formulation of perfectly elasto-plastic model is presented and the dynamic responses of the single-degree-of-freedom (s.d.o.f) viscous elasto-plastic structure under external loading is treated and the exact solutions of the responses are derived for periodic loadings. In order to give a very accurate estimation of the steady state responses, a phase-plane matching method is employed to derive essentially exact formulae, where the only approximation is finding the roots of a single transcendental algebraic equation about the elastic-phase duration variable y, which dividing by forcing frequency measures the time spent in the elastic phase per half cycle. It would be clear that all the complicated behaviour of the considered system in the low frequency ratio range can be explained by investigating the distribution of the roots of y. This exact approach makes investigation the influence of the system parameters easy. However, we warn of the possible complication of the resulting formulae due to the inclusion of the viscous damping term in the equation of motion.

2. Damped perfectly elasto-plastic structure

2.1. Equation of motion

Let us consider a s.d.o.f. structure subjected to an external loading $p(t)$. The equation of motion can be written as

$$m\ddot{x}(t) + c\dot{x}(t) + r(t) = p(t). \tag{1}$$

Here, t is time and a superposed dot represents a time differentiation; m, c and r are, respectively, the mass, damping coefficient and constitutive force of the structure; and $x(t)$ is the displacement dependent on time. This oscillator as schematically shown in Fig. 1 is called a *viscous elasto-plastic oscillator*, which comprises four parts: the mass, the viscous damping device, the elastic spring, and the Saint-Venant slider. The last two will be modelled below.

2.2. Perfectly elasto-plastic model

In this paper the *non-linearity* of the structure is reflected in a perfectly elasto-plastic model for the relationship of constitutive force and displacement, of which the following postulations are usually employed [17]:

$$\dot{x} = \dot{x}_e + \dot{x}_\mathrm{p}, \tag{2}$$

$$\dot{r} = k\dot{x}_e, \tag{3}$$

$$\dot{\lambda} r = r_y \dot{x}_\mathrm{p}, \tag{4}$$

$$|r| \leqslant r_y, \tag{5}$$

$$\dot{\lambda} \geqslant 0, \tag{6}$$

$$|r|\dot{\lambda} = r_y \dot{\lambda}. \tag{7}$$

The two constants, namely the elastic stiffness k and the yield strength r_y, are assumed to be positive. Here x, x_e, x_p and r are, respectively, the displacement, elastic displacement, plastic displacement and constitutive force; λ is a scalar called the equivalent plastic displacement, i.e., $\lambda(t) = \int_0^t |\dot{x}^p(\xi)|\,\mathrm{d}\xi$.

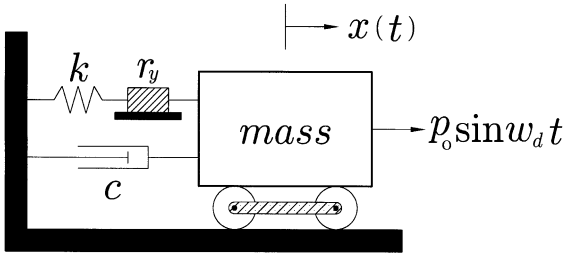

Fig. 1. Mechanical apparatus for the viscous elasto-plastic oscillator subjected to external harmonic loading.

2.3. Switch of elasticity and plasticity

Combining Eqs. (2)–(4), we have

$$\dot{r} + \frac{k}{r_y}\dot{\lambda} r = k\dot{x}, \tag{8}$$

which together with the complementary trios (5)–(7) enable the model to possess two elastic–plastic switching criteria as follows:

$$\dot{\lambda} = \frac{1}{r_y} r\,\dot{x} > 0 \text{ if } |r| = r_y \quad \text{and} \quad r\dot{x} > 0, \tag{9}$$

$$\dot{\lambda} = 0 \text{ if } |r| < r_y \text{ or } r\dot{x} \leqslant 0. \tag{10}$$

According to the complementary trios (5)–(7), there are just two *phases*: (i) $\dot{\lambda} > 0$ and $|r| = r_y$, and (ii) $\dot{\lambda} = 0$ and $|r| \leqslant r_y$. From criteria (9) and (10) it is clear that (i) corresponds to the *plastic phase*, while (ii), to the *elastic phase*.

2.4. Two-phase linear system

Note that

$$r(t) = r(t_i) \tag{11}$$

in the plastic phase, if t_i is chosen to be the switched-on time, hence, Eq. (1) becomes

$$m\ddot{x}(t) + c\dot{x}(t) = p(t) - r(t_i). \tag{12}$$

In the elastic phase, i.e., $\dot{\lambda} = 0$, Eq. (4) requires x_p to be frozen and Eqs. (2) and (3) together reduce to $\dot{r} = k\dot{x}$, integrating of which from t_i to t yields

$$r(t) = r(t_i) + k[x(t) - x(t_i)], \tag{13}$$

such that Eq. (1) changes to

$$m\ddot{x}(t) + c\dot{x}(t) + kx(t) = p(t) - r(t_i) + kx(t_i). \tag{14}$$

During the elastic phase, the motion of the viscous elasto-plastic oscillator is described by Eq. (14) supplemented with Eq. (13), and we call it *elastic motion*. Conversely, in the plastic phase the motion of the viscous elasto-plastic oscillator is governed by Eq. (12) supplemented with Eq. (11), and we call it *plastic motion*. Indeed, it is a two-phase linear system with an elastic–plastic switch to decide which motion occurs in the subsequent time interval.

3. Estimation of steady state responses

In the following the driving force is taken to be harmonic with a single driving frequency ω_d:

$$p(t) = p_0 \sin \omega_d t, \tag{15}$$

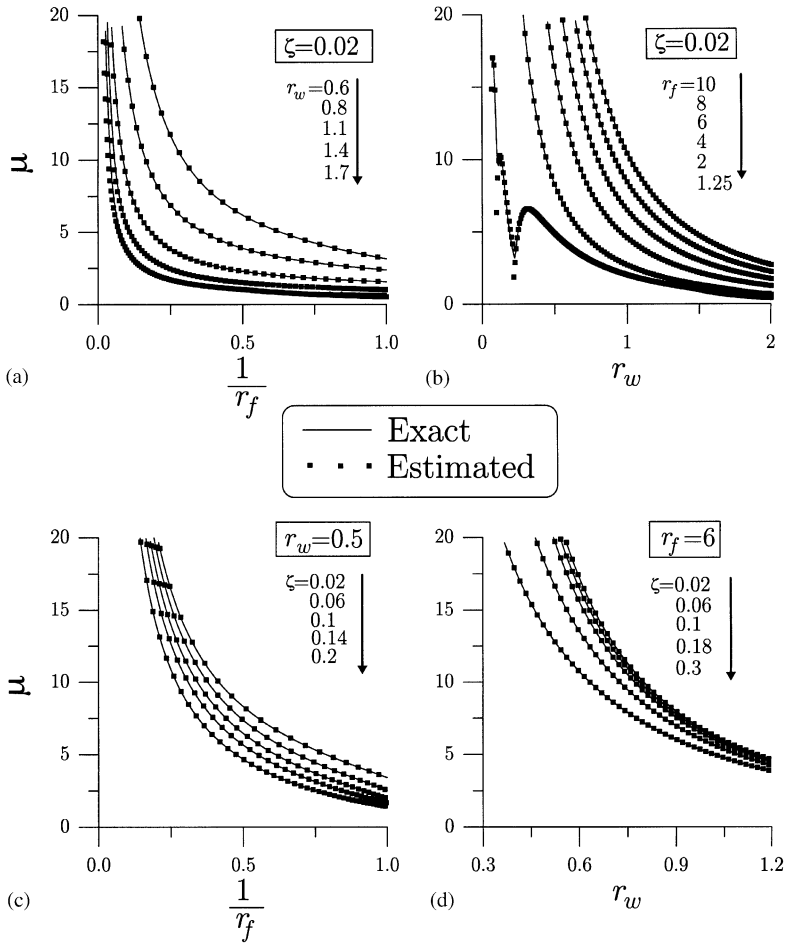

Fig. 2. The comparison of the ductility ratio between exact time-marching solution and the new estimate for (a) $\zeta = 0.02$ and five values of r_w, (b) $\zeta = 0.02$ and six values of r_f, (c) $r_w = 0.5$ and five values of ζ, and (d) $r_f = 6$ and five values of ζ: ——, exact; ▩, estimated.

where p_0 is the amplitude of periodic excitation on mass. The solutions of Eqs. (12) and (14) under the above loading are standard, which together with the determinations of phase transition points are relegated into the appendix.

For hysteretical oscillator the motion is usually transformed from one type motion to another type motion and the transitions occur frequently and regularly. The steady state analyses employed in the elastic system are no longer suitable for the dynamic analyses of the elasto-plastic system, since the frequent switch renders the responses not always to stay in one of the two motions. But, for engineering purposes we may not be especially concerned with the time histories of the responses. Rather, it is their extreme values that convey crucial information, for they are related to the maximum responses that structures must be able to endure. In this regard with the aid of the time-marching solutions we plot some extremal responses of the structure in Fig. 2 with solid lines. We let $\Delta = (x_{\max} - x_{\min})/2$ denote the oscillating amplitude in the steady state, and ζ,

r_f and r_w defined in Eqs. (A.3), (A.7) and (A.8) are, respectively, the damping ratio, force ratio and frequency ratio. For fixed value of $\zeta = 0.02$, the variations of μ with respect to $1/r_f$ are plotted in Fig. 2(a) with different $r_w(= 0.6, 0.8, 1.1, 1.4, 1.7)$. Here, $\mu := \Delta/x_y$ with $x_y = r_y/k$ is usually called the ductility ratio in the structural engineering field. They show that larger r_w leads to smaller μ. For fixed value of $\zeta = 0.02$, the variations of μ with respect to r_w are plotted in Fig. 2(b) with different $r_f(= 1.25, 2, 4, 6, 8, 10)$. They show that smaller r_f leads to smaller μ. For fixed value of $r_w = 0.5$, the variations of μ with respect to $1/r_f$ are plotted in Fig. 2(c) with different $\zeta(= 0.02, 0.06, 0.1, 0.14, 0.2)$. They show that larger ζ leads to smaller μ. For fixed value of $r_f = 6$, the variations of μ with respect to r_w are plotted in Fig. 2(d) with different $\zeta(= 0.02, 0.06, 0.1, 0.18, 0.3)$. They show that larger ζ leads to smaller μ. But for larger r_w, ζ gives little influence on μ.

After finishing the estimation of steady state responses, we will return to Fig. 2 by comparing the estimated results with that calculated from the time-marching solutions. Before doing this we first note that there are two closed loops in the steady state responses for hysteretic oscillator: hysteretic loops in the plane (x, r), and limit cycles in the plane $(x, \dot{x})$. Under what conditions of the parameters and inputs that the loops exist? Second, it can be seen that the frequency response curves as shown in Fig. 2(b) are smooth for $r_f = 2, 4, 6, 8, 10$, and when r_w approaches zero the ductility ratios (μ's) under these force ratios become unbounded, but for $r_f = 1.25$ the frequency response curve is not so smooth and exhibits several peaks, and even when r_w approaches zero the ductility ratio is bounded. Third, the mean displacement $x_m = (x_{max} + x_{min})/2$ is sensitive near the point $r_w = 0.2$. For demonstration we display two calculated examples as shown in Fig. 3 for undamped case and damped case with $\zeta = 0.02$. The response curves are subjected to the same force ratio $r_f = 1.25$ but different frequency ratios $r_w = 0.2$ (as shown with thick solid lines) and $r_w = 0.19$ (as shown with thin solid lines) in Figs. 3(a)–(d), and $\omega_d/\omega = 0.2$ (as shown with thick solid lines) and $\omega_d/\omega = 0.19$ (as shown with thin solid lines) in Figs. 3(e)–(h). It can be seen that little difference of the frequency ratio leads to very different mean displacements as shown in Figs. 3(a) and (e). However, their steady state responses are similar after a translation of displacement. This fact reveals that for the perfectly viscous elasto-plastic oscillator, we may develop estimation method for predicting the oscillation amplitude, but not for the mean displacement. We also need to mention the possible occurrence of intermediate unloadings in the steady state for certain parameters as shown in Figs. 3(c), (d), (g) and (h).

Miller and Butler [6] have demonstrated that the appearance of intermediate unloading leads to a reduction of the hysteretic loop size and a deep valley in the frequency response curve. This can be seen from Fig. 2(b), where near the point $r_w = 0.2$, the frequency response curve with $r_f = 1.25$ has a lower peak. In order to treat the intermediate unloading type behaviour in the steady state, Miller and Butler [6] and Capecchi [8] have, respectively, introduced one-dimensional iterated maps in reduced space, and asserted that the appearance of intermediate unloading at certain parametric point is closely related to the appearance of unstable fixed points at that parametric point. Below we treat these problems with a more direct method through matching the exact solutions (orbits) in the phase plane.

3.1. A phase-plane estimation

Now, let us consider a steady state motion of the viscous elasto-plastic oscillator and assume the phase curve of the steady-state motion in the phase plane $(x, \dot{x})$ to be symmetrical with respect

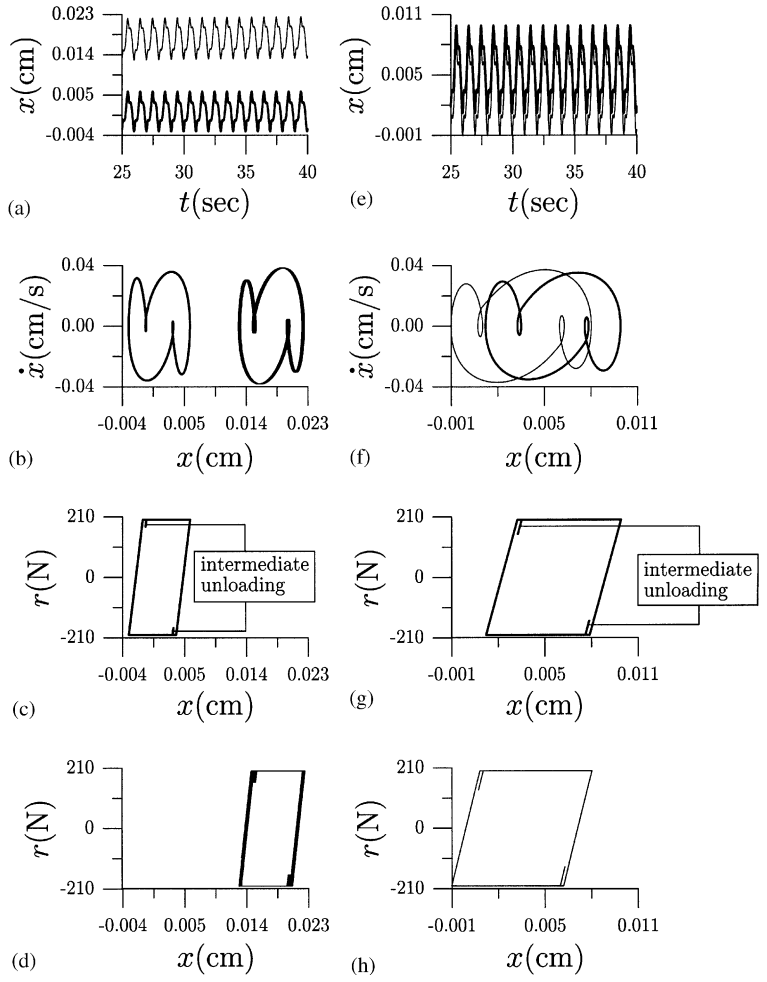

Fig. 3. Intermediate unloading motions of the viscous elasto-plastic oscillator were happened for some cases. The last 15 cycles behaviour was shown in (a)–(d), where the responses under $\zeta = 0$, $r_f = 1.25$, and $r_w = 0.2$ were presented by thick black lines, and that with the same ζ and r_f but slightly different $r_w = 0.19$ were presented by thin solid lines. The behaviour shown in (e)–(h) under $\zeta = 0.02$, $r_f = 1.25$, and $\omega_d/\omega = 0.2$ were presented by thick black lines, and that with the same ζ and r_f but slightly different $\omega_d/\omega = 0.19$ were presented by thin solid lines.

to the point $(x_m, 0)$, where x_m is the mean of the displacement in the steady state. Therefore, the phase curve is closed in the phase plane and it suffices to consider only one half of the curve, say the upper branch. Referring to Fig. 4(a), let $x_m + \Delta$ denote the maximum displacement of the steady state motion, t_2 the transition time between elastic motion and plastic motion, and t_1 the starting time of elastic motion, so as to match the exact solutions of the steady state response of the viscous elasto-plastic oscillator. Because of the periodicity of the input and the symmetry with respect to $(x_m, 0)$ of the steady state motion, we may assume

$$t_3 = t_1 + \frac{\pi}{\omega_d}, \tag{16}$$

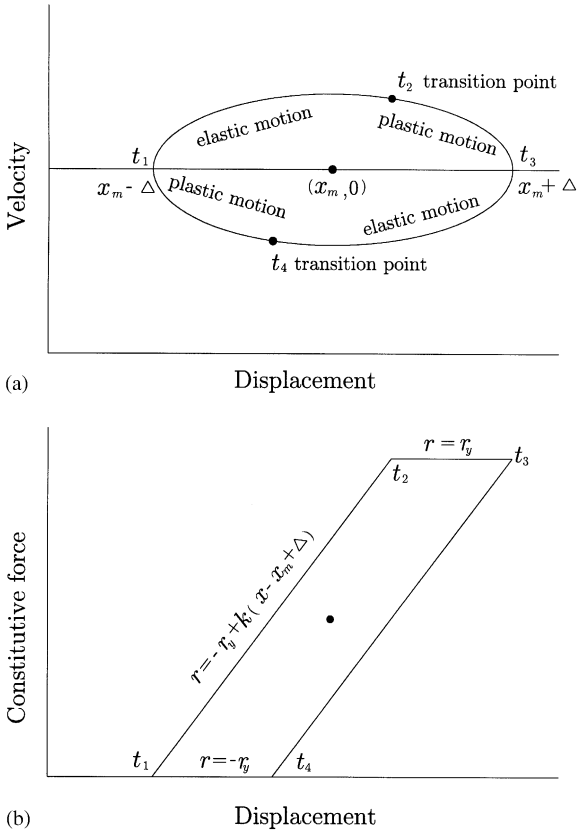

Fig. 4. A typical steady state response with (a) limit cycle in the displacement–velocity phase plane, (b) dissipation loop in the displacement-constitutive force plane; t_1, t_2, and Δ are all to be determined.

and estimate the three parameters, namely the amplitude of displacement Δ, and the time lags t_1 and t_2.

In the time interval $t_1 \leqslant t \leqslant t_2$, the constitutive force in view of Fig. 4(b) is given by

$$r = -r_y + k(x - x_{\mathrm{m}} + \Delta).$$

Substituting it into Eq. (1), we obtain

$$m\ddot{x}(t) + c\dot{x}(t) + kx(t) = r_y + k(x_{\mathrm{m}} - \Delta) + p_0 \sin \omega_{\mathrm{d}} t, \tag{17}$$

whose solution, upon considering the following conditions at $t = t_1$,

$$x_1(t_1) = x_{\mathrm{m}} - \Delta, \quad \dot{x}_1(t_1) = 0 \tag{18, 19}$$

is found to be

$$\begin{aligned} x_1(t) = {} & \exp[-\zeta\omega_n(t - t_1)][C_1 \cos \omega(t - t_1) + C_2 \sin \omega(t - t_1)] \\ & + A_1 \sin \omega_{\mathrm{d}} t - B_1 \cos \omega_{\mathrm{d}} t + x_y + x_{\mathrm{m}} - \Delta. \end{aligned} \tag{20}$$

Here C_1 and C_2 as defined in Eqs. (A.10) and (A.11) are now replaced, respectively, by

$$C_1 \coloneqq B_1 \cos \omega_d t_1 - A_1 \sin \omega_d t_1 - x_y, \tag{21}$$

$$C_2 \coloneqq \frac{[B_1\zeta - A_1 r_w]\cos \omega_d t_1}{\sqrt{1-\zeta^2}} - \frac{[B_1 r_w + A_1\zeta]\sin \omega_d t_1}{\sqrt{1-\zeta^2}} - \frac{\zeta x_y}{\sqrt{1-\zeta^2}}. \tag{22}$$

Similarly, solving Eq. (1) with its $r(t)$ replaced by r_y, and using the following conditions at $t = t_3$,

$$x_2(t_3) = x_m + \Delta, \quad \dot{x}_2(t_3) = 0, \tag{23, 24}$$

$x_2(t)$ in the time interval $t_2 \leqslant t \leqslant t_3$ can be derived

$$x_2(t) = C_4 + C_3 \exp[-2\zeta\omega_n(t - t_3)] - A_2 \sin \omega_d t - B_2 \cos \omega_d t - \frac{r_y}{c}t, \tag{25}$$

where C_3 and C_4 as defined in Eqs. (A.15) and (A.16) are now replaced, respectively, by

$$C_3 \coloneqq A_2 \sin \omega_d t_3 - \frac{r_w}{2\zeta}A_2 \cos \omega_d t_3 - \frac{x_y}{4\zeta^2}, \tag{26}$$

$$C_4 \coloneqq \left[B_2 + \frac{r_w}{2\zeta}A_2\right]\cos \omega_d t_3 + \frac{r_y}{2\zeta\omega_n c} + \frac{t_3 r_y}{c} + x_m + \Delta. \tag{27}$$

Both the constitutive force $r(t)$ and the external force $p(t)$ are continuous at the transition time t_2 between the elastic motion and the plastic motion, which due to Eq. (1) renders the acceleration $\ddot{x}(t)$ to be continuous at the transition time t_2. The continuities of $\dot{x}$ and x are obvious for they are integrations of $\ddot{x}$ and $\dot{x}$, respectively. Thus with Eqs. (20), (25) and (16) the following three conditions:

$$x_1(t_2) = x_2(t_2), \quad \dot{x}_1(t_2) = \dot{x}_2(t_2), \quad \ddot{x}_1(t_2) = \ddot{x}_2(t_2) \tag{28–30}$$

become the following three equations:

$$\exp\left[\frac{-\zeta y}{r_w}\right](C_1 \cos \bar{y} + C_2 \sin \bar{y}) + (A_1 + A_2)\sin \omega_d t_2 + (B_2 - B_1)\cos \omega_d t_2 - A_2 \sin \omega_d t_2 - B_2 \cos \omega_d t_2 + C_3\left(1 - \exp\left[\frac{2\zeta(\pi - y)}{r_w}\right]\right) - \frac{r_y}{c\omega_d}(\pi - y) - 2\Delta = 0, \tag{31}$$

$$-\zeta\omega_n \exp\left[\frac{-\zeta y}{r_w}\right](C_1 \cos \bar{y} + C_2 \sin \bar{y}) + (A_1 + A_2)\omega_d \cos \omega_d t_2 + (B_1 - B_2)\omega_d \sin \omega_d t_2 + \omega \exp\left[\frac{-\zeta y}{r_w}\right](C_2 \cos \bar{y} - C_1 \sin \bar{y}) + \frac{r_y}{c} + 2C_3\zeta\omega_n \exp\left[\frac{2\zeta(\pi - y)}{r_w}\right] = 0, \tag{32}$$

$$(\zeta^2\omega_n^2 - \omega^2)\exp\left[\frac{-\zeta y}{r_w}\right](C_1 \cos \bar{y} + C_2 \sin \bar{y}) - 2\zeta\omega_n\omega \exp\left[\frac{-\zeta y}{r_w}\right](C_2 \cos \bar{y} - C_1 \sin \bar{y}) - (A_1 + A_2)\omega_d^2 \sin \omega_d t_2 + (B_2 - B_1)\omega_d^2 \cos \omega_d t_2 - 4C_3\zeta^2\omega_n^2 \exp\left[\frac{2\zeta(\pi - y)}{r_w}\right] = 0, \tag{33}$$

where

$$y \coloneqq \omega_d(t_2 - t_1), \quad 0 < y \leqslant \pi, \tag{34}$$

$$\bar{y} \coloneqq \frac{\sqrt{1-\zeta^2}}{r_w}y = \omega(t_2 - t_1). \tag{35}$$

y may be called the elastic-phase duration variable, which when divided by forcing frequency measures the time spent in the elastic phase per half cycle.

Even though we have taken x_m into the consideration at the beginning, fortunately all these x_m's cancel out and hence the resulting Eqs. (31)–(33) are independent of x_m. In principle, we can combine the three Eqs. (31)–(33) together utilizing numerical method to determine the three unknowns t_1, t_2, and Δ. However, these equations are too complicated to give us proper information about t_1, t_2, and Δ and the influence of parameters values on them. Below we put these equations into a more concise form such that in terms of the identified parameters the closed-form representations of t_1, t_2, and Δ are available.

3.2. Closed-form formula for force ratio

In Eqs. (32) and (33) if we replace $\cos\omega_d t_2$ and $\sin\omega_d t_2$, respectively, by

$$\cos\omega_d t_2 = \cos y\cos\omega_d t_1 - \sin y\sin\omega_d t_1, \tag{36}$$

$$\sin\omega_d t_2 = \sin y\cos\omega_d t_1 + \cos y\sin\omega_d t_1, \tag{37}$$

we obtain the simultaneous equations for $\cos\omega_d t_1$ and $\sin\omega_d t_1$:

$$\hat{a}\cos\omega_d t_1 + \hat{b}\sin\omega_d t_1 = \hat{c}, \tag{38}$$

$$\hat{d}\cos\omega_d t_1 + \hat{e}\sin\omega_d t_1 = \hat{f}, \tag{39}$$

where $\hat{a}$, $\hat{b}$, $\hat{c}$, $\hat{d}$, $\hat{e}$, and $\hat{f}$ are dimensionless coefficients given by

$$\begin{aligned}\hat{a} \coloneqq{}& (\hat{A}_1+\hat{A}_2)r_w\cos y + (\hat{B}_1-\hat{B}_2)r_w\sin y - \exp\left[\frac{-\zeta y}{r_w}\right]\hat{A}_1 r_w\cos\bar{y}\\ &+\exp\left[\frac{-\zeta y}{r_w}\right]\frac{\zeta r_w\hat{A}_1-\hat{B}_1}{\sqrt{1-\zeta^2}}\sin\bar{y} + \exp\left[\frac{2\zeta(\pi-y)}{r_w}\right]\hat{A}_2 r_w,\end{aligned} \tag{40}$$

$$\begin{aligned}\hat{b} \coloneqq{}& -(\hat{A}_1+\hat{A}_2)r_w\sin y + (\hat{B}_1-\hat{B}_2)r_w\cos y - \exp\left[\frac{-\zeta y}{r_w}\right]\hat{B}_1 r_w\cos\bar{y}\\ &+\exp\left[\frac{-\zeta y}{r_w}\right]\frac{\hat{A}_1+\zeta r_w\hat{B}_1}{\sqrt{1-\zeta^2}}\sin\bar{y} - \exp\left[\frac{2\zeta(\pi-y)}{r_w}\right]\hat{B}_2 r_w,\end{aligned} \tag{41}$$

$$\hat{c} \coloneqq -\exp\left[\frac{-\zeta y}{r_w}\right]\frac{1}{\sqrt{1-\zeta^2}}\sin\bar{y} + \frac{1}{2\zeta}\left(\exp\left[\frac{2\zeta(\pi-y)}{r_w}\right]-1\right), \tag{42}$$

$$\begin{aligned}\hat{d} \coloneqq{}& \exp\left[\frac{-\zeta y}{r_w}\right]\frac{\zeta\hat{B}_1 + r_w(1-2\zeta^2)\hat{A}_1}{\sqrt{1-\zeta^2}}\sin\bar{y} + \exp\left[\frac{-\zeta y}{r_w}\right](2\zeta r_w\hat{A}_1-\hat{B}_1)\cos\bar{y}\\ &-r_w^2(\hat{A}_1+\hat{A}_2)\sin y + r_w^2(\hat{B}_1-\hat{B}_2)\cos y - 2\zeta r_w\hat{A}_2\exp\left[\frac{2\zeta(\pi-y)}{r_w}\right],\end{aligned} \tag{43}$$

$$\hat{e} \coloneqq \exp\left[\frac{-\zeta y}{r_w}\right]\frac{r_w(1-2\zeta^2)\hat{B}_1 - \zeta\hat{A}_1}{\sqrt{1-\zeta^2}}\sin\bar{y} + \exp\left[\frac{-\zeta y}{r_w}\right](\hat{A}_1 + 2\zeta r_w\hat{B}_1)\cos\bar{y}$$
$$- r_w^2(\hat{A}_1 + \hat{A}_2)\cos y + r_w^2(\hat{B}_2 - \hat{B}_1)\sin y + 2\zeta r_w\hat{B}_2\exp\left[\frac{2\zeta(\pi - y)}{r_w}\right], \tag{44}$$

$$\hat{f} \coloneqq -\exp\left[\frac{-\zeta y}{r_w}\right]\cos\bar{y} + \exp\left[\frac{-\zeta y}{r_w}\right]\frac{\zeta}{\sqrt{1-\zeta^2}}\sin\bar{y} - \exp\left[\frac{2\zeta(\pi - y)}{r_w}\right], \tag{45}$$

in which

$$\hat{A}_1 \coloneqq \frac{r_f(1-r_w^2)}{(1-r_w^2)^2 + 4\zeta^2 r_w^2}, \tag{46}$$

$$\hat{B}_1 \coloneqq \frac{2\zeta r_f r_w}{(1-r_w^2)^2 + 4\zeta^2 r_w^2}, \tag{47}$$

$$\hat{A}_2 \coloneqq \frac{r_f}{r_w^2 + 4\zeta^2}, \tag{48}$$

$$\hat{B}_2 \coloneqq \frac{2\zeta r_f}{r_w(r_w^2 + 4\zeta^2)}. \tag{49}$$

Solving $\cos\omega_d t_1$ and $\sin\omega_d t_1$ from Eqs. (38) and (39), we obtain

$$\cos\omega_d t_1 \coloneqq \frac{\hat{c}\hat{e} - \hat{b}\hat{f}}{\hat{a}\hat{e} - \hat{b}\hat{d}}, \tag{50}$$

$$\sin\omega_d t_1 \coloneqq \frac{\hat{a}\hat{f} - \hat{c}\hat{d}}{\hat{a}\hat{e} - \hat{b}\hat{d}}. \tag{51}$$

Substituting them into the identity $\cos^2\omega_d t_1 + \sin^2\omega_d t_1 = 1$, we obtain a single equation

$$(\hat{c}\hat{e} - \hat{b}\hat{f})^2 + (\hat{a}\hat{f} - \hat{c}\hat{d})^2 = (\hat{a}\hat{e} - \hat{b}\hat{d})^2. \tag{52}$$

Solving Eq. (52) for r_f we obtain

$$r_f = \sqrt{\frac{(\hat{c}\bar{e} - \bar{b}\hat{f})^2 + (\bar{a}\hat{f} - \hat{c}\bar{d})^2}{[\bar{a}\bar{e} - \bar{b}\bar{d}]^2}}, \tag{53}$$

where $\bar{a}$, $\bar{b}$, $\bar{d}$, and $\bar{e}$ are given by the ones defined, respectively, in Eq. (40), (41), (43) and (44) but their $\hat{A}_1$, $\hat{B}_1$, $\hat{A}_2$ and $\hat{B}_2$ replaced, respectively, by the following $\bar{A}_1$, $\bar{B}_1$, $\bar{A}_2$ and $\bar{B}_2$:

$$\bar{A}_1 \coloneqq \frac{1-r_w^2}{(1-r_w^2)^2 + 4\zeta^2 r_w^2}, \tag{54}$$

$$\bar{B}_1 \coloneqq \frac{2\zeta r_w}{(1-r_w^2)^2 + 4\zeta^2 r_w^2} = \frac{2\zeta r_w}{1-r_w^2}\bar{A}_1, \tag{55}$$

$$\bar{A}_2 := \frac{1}{r_w^2 + 4\zeta^2}, \tag{56}$$

$$\bar{B}_2 := \frac{2\zeta}{r_w(r_w^2 + 4\zeta^2)} = \frac{2\zeta}{r_w}\bar{A}_2. \tag{57}$$

Up to now we have combined three highly transcendental algebraic Eqs. (31)–(33) into a single scalar equation (53), which specifies the function/relationship of $r_f = r_f(\zeta, r_w, y)$ in the steady state. Applying numerical method to the function $r_f = r_f(\zeta, r_w, y)$, we can build up the inverse relation $y = y(\zeta, r_w, r_f)$, and as to be done below, the variation of the ductility ratio in terms of ζ, r_w and r_f can be evaluated.

Now we can define the relation between of the elastic-duration variable y and the other parameters. For each fixed ζ and r_w, we plot the relation between $1/r_f$ and y via Eq. (53) by letting y to vary in the range $(0, \pi]$. This relation, as shown in Fig. 5(a) which gives curves $1/r_f$ versus y with $\zeta = 0.02$ and $r_w = 1.7, 1.4, 1.1, 0.8, 0.6$, is homeomorphic, i.e., $d(1/r_f)/dy > 0$, i.e., $dr_f/dy < 0$. More precisely, the relation of r_f and y is one-to-one and onto.

Conversely, given r_f and ζ we need to solve Eq. (53) for giving the relation between r_w and y. Numerically solving y from Eq. (53) is quite simple, and the calculation can be performed to arbitrary accuracy. In practice the error tolerance used in finding the roots is 10^{-10}. We may fix r_f within the interval $[\sqrt{(1 - r_w^2)^2 + (2\zeta r_w)^2}, \infty)$. When $r_f < \sqrt{(1 - r_w^2)^2 + (2\zeta r_w)^2}$ we can prove

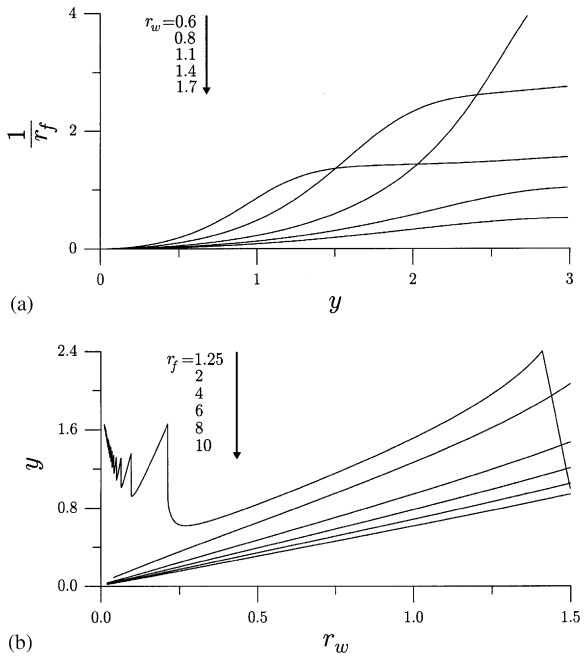

Fig. 5. (a) The force ratio r_f is homeomorphic with y when r_w is fixed; we plot the variation of $1/r_f$ with respect to y for five values of r_w. (b) Conversely, when r_f is fixed we need to solve y from Eq. (53) for giving the variation of y with respect to r_w for six values of r_f. Only the smallest root of y is presented here.

that the structure is in elastic shakedown, and we search for the relation between r_w and y as shown in Fig. 5(b) with $\zeta = 0.02$ and $r_f = 1.25, 2, 4, 6, 8, 10$. Here only the smallest solutions of y were plotted. It can be seen that the curves with $r_f = 2, 4, 6, 8, 10$ are smooth for all r_w in the range $(0, 1.5]$, but the one with $r_f = 1.25$ are oscillatory, non-smooth, and having jump in the low frequency ratio range.

3.3. Closed-form formula for ductility ratio

In Eq. (31) if we substitute Eq. (36) for $\cos\omega_d t_2$ and Eq. (37) for $\sin\omega_d t_2$, and then replace $\cos\omega_d t_1$ and $\sin\omega_d t_1$, respectively, by Eqs. (50) and (51) but with their $\hat{a}$, $\hat{b}$, $\hat{d}$, and $\hat{e}$ replaced, respectively, by $\bar{a}$, $\bar{b}$, $\bar{d}$, and $\bar{e}$, we obtain a closed-form representation of μ:

$$
\begin{aligned}
2\mu = {} & \left(\frac{\hat{c}\bar{e} - \bar{b}\hat{f}}{\bar{a}\bar{e} - \bar{b}\bar{d}}\right)\left\{\exp\left[\frac{-\zeta y}{r_w}\right]\left[\frac{\zeta\bar{B}_1 - r_w\bar{A}_1}{\sqrt{1-\zeta^2}}\sin\bar{y} + \bar{B}_1\cos\bar{y}\right] + (\bar{A}_1 + \bar{A}_2)\sin y\right. \\
& \left. + (\bar{B}_2 - \bar{B}_1)\cos y + \frac{r_w\bar{A}_2}{2\zeta}\left(1 - \exp\left[\frac{2\zeta(\pi - y)}{r_w}\right]\right) + \bar{B}_2\right\} \\
& + \left(\frac{\bar{a}\hat{f} - \hat{c}\bar{d}}{\bar{a}\bar{e} - \bar{b}\bar{d}}\right)\left\{\exp\left[\frac{-\zeta y}{r_w}\right]\left[\frac{\zeta\bar{A}_1 + r_w\bar{B}_1}{\sqrt{1-\zeta^2}}\sin\bar{y} + \bar{A}_1\cos\bar{y}\right] + (\bar{A}_1 + \bar{A}_2)\cos y\right. \\
& \left. + (\bar{B}_1 - \bar{B}_2)\sin y - \frac{r_w\bar{B}_2}{2\zeta}\left(1 - \exp\left[\frac{2\zeta(\pi - y)}{r_w}\right]\right) - \bar{A}_2\right\} + 1 - \frac{\pi - y}{2\zeta r_w} \\
& - \exp\left[\frac{-\zeta y}{r_w}\right]\left[\cos\bar{y} + \frac{\zeta}{\sqrt{1-\zeta^2}}\sin\bar{y}\right] + \frac{1}{4\zeta^2}\left(\exp\left[\frac{2\zeta(\pi - y)}{r_w}\right] - 1\right).
\end{aligned} \tag{58}
$$

It can be seen that μ depends explicitly on three parameters ζ, r_w and y, and its dependence on ζ, r_w and r_f can be realized through the relation $y = y(\zeta, r_w, r_f)$.

We are interested to know the variation of μ with respect to r_f as well as to r_w for some fixed values of ζ. For fixed values of ζ and r_w, the variation of μ with respect to r_f can be evaluated by substituting the y's in Fig. 5(a) into Eq. (58). The response curves are shown in Fig. 2(a) with solid square black points for $\zeta = 0.02$ and $r_w = 0.6, 0.8, 1.1, 1.4, 1.7$. Conversely, substituting the y's in Fig. 5(b) into Eq. (58) the variation of μ with respect to r_w are plotted for $\zeta = 0.02$ and $r_f = 1.25, 2, 4, 6, 8, 10$ as shown in Fig. 2(b) with solid square black points. Similarly, the variations of μ with respect to $1/r_f$ are displayed in Fig. 2(c) with solid square black points for $r_w = 0.5$ and $\zeta = 0.02, 0.06, 0.1, 0.14, 0.2$. The variations of μ with respect to r_w are displayed in Fig. 2(d) with solid square black points for $r_f = 6$ and $\zeta = 0.02, 0.06, 0.1, 0.18, 0.3$.

Now we compare the estimated results (marked with solid square black points) with the exact results (displayed with solid lines) calculated by the exact time-marching solutions as shown in Eqs. (A.1) and (A.12) for different r_w's in Fig. 2(a), for different r_f's in Fig. 2(b) and for different ζ's in Figs. 2(c) and 2(d). From these four plots we confirm that formula (58) is very accurate to estimate the oscillating amplitude of the viscous elasto-plastic oscillator in the steady state.

The ductility ratio is an important factor that influences the selection of suitable yield strength of the structure. We usually require the ductility ratio must to be smaller than the design ductility ratio, and such that the structure can survive without failure when subjected to certain external

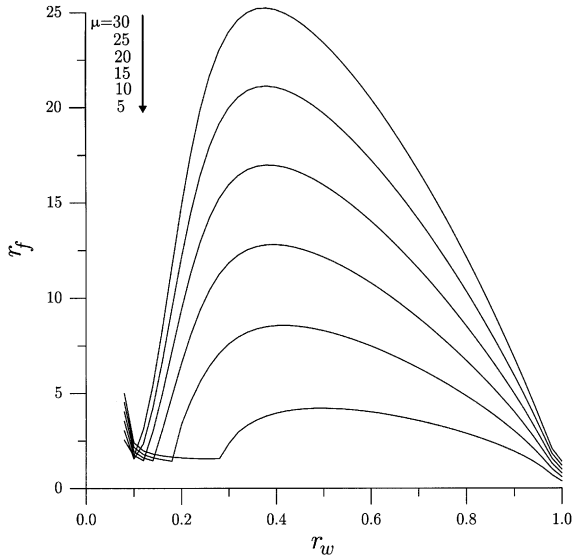

Fig. 6. The frequency response curves with specified ductility ratios $\mu = 5, 10, 15, 20, 25, 30$.

loading. Now, we fix the value of μ and attempt to search for the relation between r_f and r_w that renders the structures able to respond with such μ. Given μ, we solve y from Eq. (58) by letting r_w to vary. Then by substituting the above y's and r_w into Eq. (53), we can obtain the curves of r_f versus r_w as shown in Fig. 6 for different $\mu(= 5, 10, 15, 20, 25, 30)$.

3.4. Dissipation loop size

For the engineering purpose we may deal with the energy dissipation capacity of the structure considered. From Fig. 4(b) the area of energy dissipation loop is found to be

$$\ell_a = 4r_y(\Delta - x_y), \tag{59}$$

and thus with the help of Eq. (58) we can assess the influence of the two system parameters r_f and r_w on ℓ_a. For this purpose let us introduce the following two dimensionless variables for the size of the dissipation loop:

$$\Lambda_1 := \frac{k\ell_a}{p_0^2} = \frac{4}{r_f^2}(\mu - 1), \tag{60}$$

$$\Lambda_2 := \frac{m\omega_d^2\ell_a}{p_0^2} = \frac{4r_w^2}{r_f^2}(\mu - 1). \tag{61}$$

Now some remarks on the above two formulae: (i) The left-hand side of the first equation may be understood as the dissipation per unit elastic energy, since p_0/k is the static displacement of the elastic response and p_0^2/k is the elastic energy. (ii) The factor $\mu - 1$ on the right-hand side of the first equation decreases with respect to $1/r_f$ for each r_w as shown in Fig. 2(a); conversely, the factor $1/r_f^2$ increases with respect to $1/r_f$. Therefore, there exists a best r_f to maximize Λ_1 for each r_w. (iii) Assuming $m\omega_d^2 := k_d$, the left-hand side of the second equation may be written as

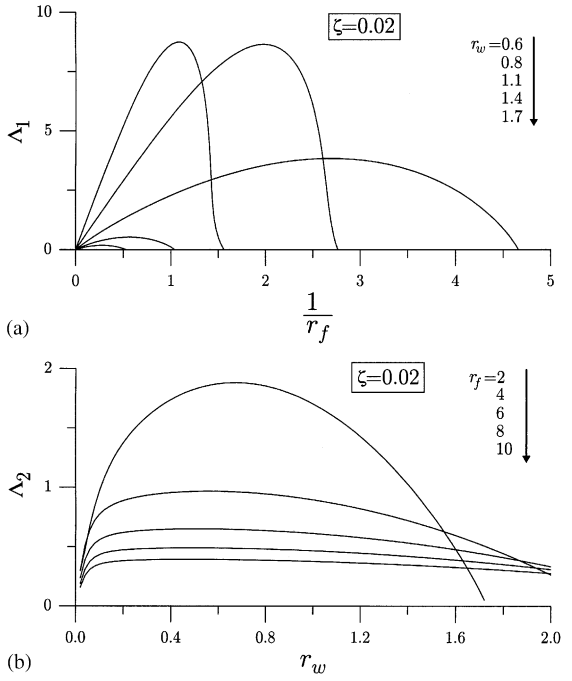

Fig. 7. (a) The variation of dimensionless dissipation loop size Λ_1 with respect to $1/r_f$ for $\zeta = 0.02$ and five values of r_w. (b) The variation of the dimensionless dissipation loop size Λ_2 with respect to r_w for $\zeta = 0.02$ and five values of r_f.

$\ell_a/(p_0^2/k_d)$. Corresponding to (i), it may be understood as the dissipation per pseudo elastic energy with a pseudo elastic stiffness k_d. (iv) The term $\mu - 1$ on the right-hand side of the second equation is known to be decreased with respect to r_w for each r_f as shown in Fig. 2(b); nevertheless, the term r_w^2 is increased with respect to r_w. Hence, there exists one best r_w to maximize Λ_2 for each r_f.

Eq. (60) is used to investigate the variation of the dimensionless size of the dissipation loop with respect to r_f. In Fig. 7(a) the variations of Λ_1 with respect to $1/r_f$ are plotted for $\zeta = 0.02$ and $r_w = 0.6, 0.8, 1.1, 1.4, 1.7$. For the purpose of isolating the building structure, we usually choose the best r_f to maximize the dissipation loop size. Under this r_f the isolator will achieve the best performance, dissipates as much energy as it can. Similarly, Eq. (61) is used to investigate the variation of the dimensionless size of the dissipation loop with respect to r_w. In Fig. 7(b) variations of Λ_2 with respect to r_w are plotted for $\zeta = 0.02$ and $r_f = 2, 4, 6, 8, 10$. For the isolation purpose, we may choose the best r_w, the r_w that maximizes the dissipation loop size.

3.5. Elastic shakedown boundary

In the case of cyclic loadings the magnitude of the input is not merely a factor characterizing the structural safety. These loads may also result in alternating plastic displacement, which after a sufficient number of cycles may cause low cycle fatigue and failure of the structure. Therefore, the structural safety requires that the plastic displacement increments due to consecutive load changes should eventually cease, the structural response of further cycles being fully elastic. Such a stabilization of plastic displacements is called (elastic) shakedown or adaptation. Thus, for the

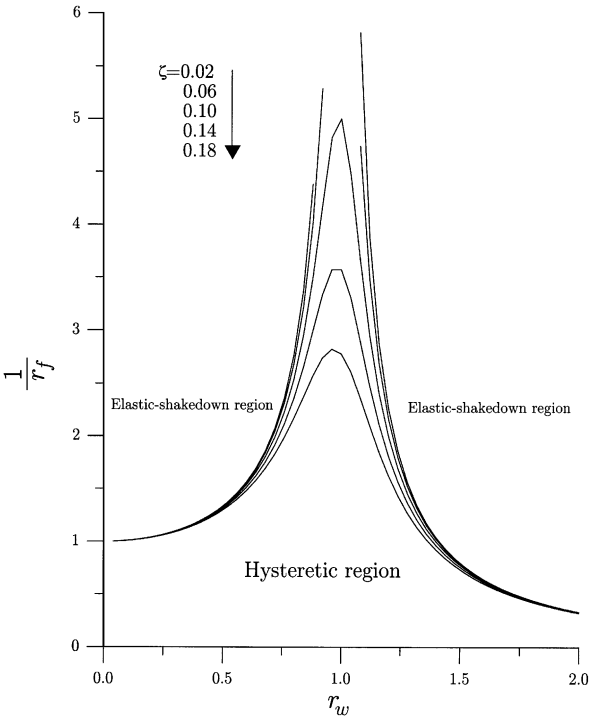

Fig. 8. The boundary curves of elastic shakedown region and hysteretic region for different damping ratios $\zeta(= 0.02, 0.06, 0.1, 0.14, 0.18)$.

purpose of safety we may hope the structure tend to elastic shakedown gradually, without inducing further plastic deformation to cause failure of the structure.

Elastic shakedown requires that the plastic dissipating loop as shown in Fig. 4(a) disappears eventually, which is equivalent to the requirement that $t_3 = t_2 = t_1 + \pi/\omega_d$ or $y = \pi$ via Eq. (34). Under this condition, by Eqs. (58) and (59), it is obvious that

$$\mu = 1, \quad \ell_a = 0, \tag{62, 63}$$

the latter of which indicates that the size of the dissipation loop is zero.

Let $y = \pi$ in Eq. (53). We can then compute the boundary curves of elastic shakedown region in the plane $(r_w, 1/r_f)$ as shown in Fig. 8 for different $\zeta(= 0.02, 0.06, 0.1, 0.14, 0.18)$. As can be seen the hysteretic region below the boundary curve reduces when the damping ratio increases.

On the other hand, we know that the elastic structure under the sinusoidal loading (15) has the following steady state oscillation amplitude:

$$\frac{x_{max}}{x_y} = \frac{r_f}{\sqrt{(1 - r_w^2)^2 + (2\zeta r_w)^2}}. \tag{64}$$

Let

$$x_{max} = x_y.$$

Then, we obtain

$$r_{\mathrm{f}} = \sqrt{(1 - r_{\mathrm{w}}^2)^2 + (2\zeta r_{\mathrm{w}})^2}. \tag{65}$$

The force ratio larger than the above value will render the restoring force of the structure exceed its elastic limit r_y, and hence elastic shakedown is impossible. The above formula gives the same curves in the plane $(r_{\mathrm{w}}, 1/r_{\mathrm{f}})$ as that calculated from Eq. (53) with $y = \pi$.

The right-hand side of Eq. (65) supplies a lower bound of r_{f} for elastic shakedown. The loading with its r_{f} smaller than the lower bound will render the response to tend to elastic shakedown. Thus, the criteria for elastic shakedown are obtained as follows:

$$r_{\mathrm{f}} < \sqrt{(1 - r_{\mathrm{w}}^2)^2 + (2\zeta r_{\mathrm{w}})^2}, \tag{66}$$

or

$$r_{\mathrm{w}} > \sqrt{1 - 2\zeta^2 + \sqrt{(1 - 2\zeta^2)^2 + r_{\mathrm{f}}^2 - 1}}. \tag{67}$$

The determination of the control parameters allowing the adaptation is one of the main goals of the plasticity theory of shakedown. Here, Eq. (66) gives a constraint on parameter values, under which the steady state response is elastic shakedown.

3.6. Undamped case

Although Eqs. (53) and (58) are applicable to the undamped case but many works needed to take account of the "0/0 terms" that appear in the coefficient functions through l'Hôspital's rule, we prefer to write down these formulae directly as follows [9]:

$$r_{\mathrm{f}} = \sqrt{\frac{(\tilde{c}\tilde{e} - \tilde{b}\tilde{f})^2 + (\tilde{a}\tilde{f} - \tilde{b}\tilde{c})^2}{[\tilde{a}\tilde{e} - \tilde{b}^2]^2}}, \tag{68}$$

$$2\mu = \frac{1}{r_{\mathrm{w}}^2}(1 + \cos y)\frac{\tilde{a}\tilde{f} - \tilde{b}\tilde{c}}{\tilde{a}\tilde{e} - \tilde{b}^2} + \frac{1}{r_{\mathrm{w}}^2}(y + \sin y - \pi)\frac{\tilde{c}\tilde{e} - \tilde{b}\tilde{f}}{\tilde{a}\tilde{e} - \tilde{b}^2} + \frac{1}{2r_{\mathrm{w}}^2}(y - \pi)^2 + 2, \tag{69}$$

where

$$\tilde{a} := r_{\mathrm{w}}^2 + r_{\mathrm{w}}^2 \cos\frac{y}{r_{\mathrm{w}}} - (1 + \cos y), \tag{70}$$

$$\tilde{b} := \sin y - r_{\mathrm{w}} \sin\frac{y}{r_{\mathrm{w}}}, \tag{71}$$

$$\tilde{c} := r_{\mathrm{w}}(1 - r_{\mathrm{w}}^2)\left[\sin\frac{y}{r_{\mathrm{w}}} + \frac{y}{r_{\mathrm{w}}} - \frac{\pi}{r_{\mathrm{w}}}\right], \tag{72}$$

$$\tilde{e} := \cos y - \cos\frac{y}{r_{\mathrm{w}}}, \tag{73}$$

$$\tilde{f} := (1 - r_{\mathrm{w}}^2)\left(1 + \cos\frac{y}{r_{\mathrm{w}}}\right). \tag{74}$$

Note that the denominator $\tilde{a}\tilde{e} - \tilde{b}^2$ approaches zero when y tends to zero. Comparing the above equations with Eqs. (53) and (58) and studying the coefficients in Eqs. (40)–(45) reveals that the inclusion of the damping term in the oscillator greatly complicates the resulting formulae. In the later we can see that the influence of the damping effect on the steady state behaviour is profound.

3.7. Intermediate unloading motions

In order to decide which parametric point in the parametric space (ζ, r_w, r_f) corresponding to periodic motion with or without intermediate unloading, let us first return to Eq. (68) for the undamped case. As in Fig. 5(b), we search the relation between r_w and y for fixed r_f. The results are plotted in Figs. 9(a) and 9(b) for $r_f = 2$ and $r_f = 1.25$, respectively. All admissible roots of y in the range $(0, \pi]$ are displayed. It can be seen that when $r_w > 1/3$ there exists only one root of y, and when r_w decreases there are more and more roots of y for both cases. The one root of y corresponds to the periodic motion without intermediate unloading, while multiple root of y indicates that the oscillator motion is periodic with intermediate unloading at such parametric point.

The curve composed of smallest root of y is smooth for $r_f = 2$ and approaches to zero when r_w approaches to zero. This explains the reason that the steady state response is unbounded when

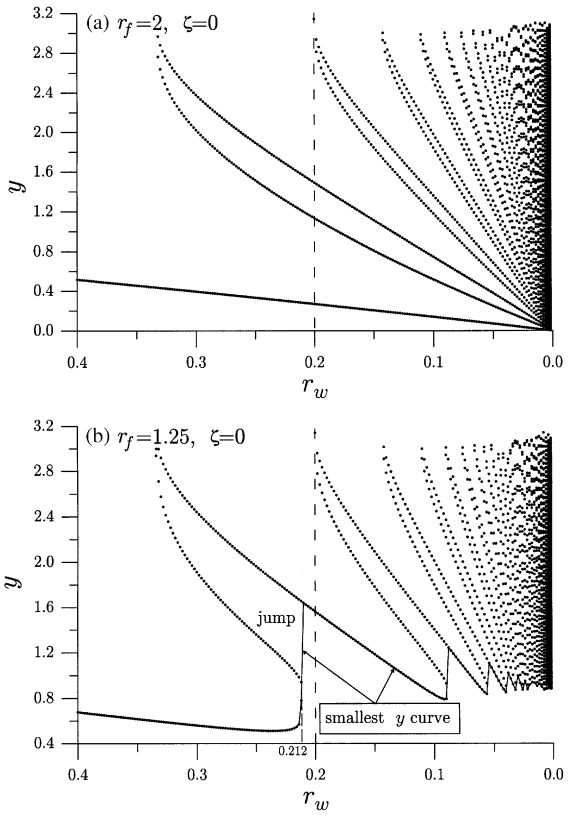

Fig. 9. All admissible roots of y are displayed for two cases: (a) $r_f = 2$ and $\zeta = 0$, and (b) $r_f = 1.25$ and $\zeta = 0$. The smallest y curve is continuous for larger r_f, but discontinuous and oscillatory for smaller r_f.

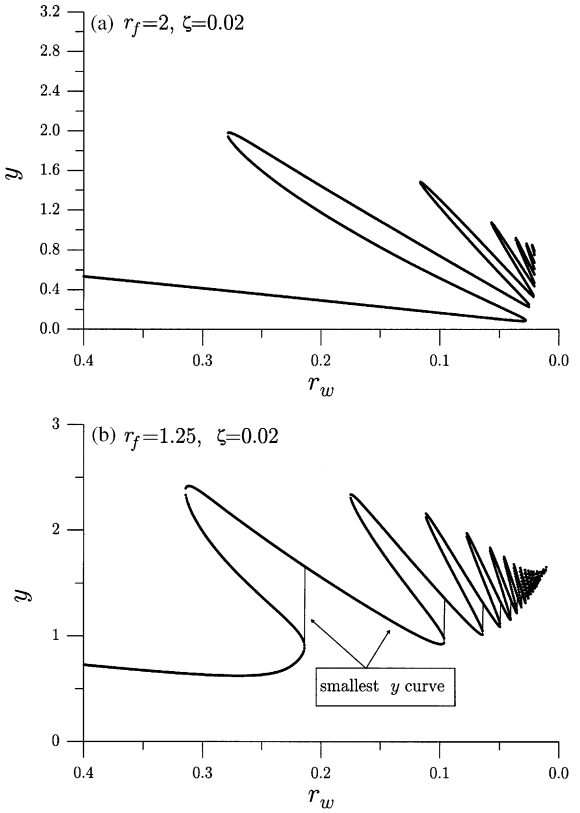

Fig. 10. All admissible roots of y are displayed for two cases: (a) $r_f = 2$ and $\zeta = 0.02$, (b) $r_f = 1.25$ and $\zeta = 0.02$. The smallest y curve is continuous for larger r_f, but discontinuous and oscillatory for smaller r_f.

$r_f = 2$, because substituting $y = 0$ into Eq. (69) will give an unbounded μ. Conversely, the smallest y curve as shown in Fig. 9(b) is non-smooth exhibiting jump for $r_f = 1.25$, and it tends to a non-zero y when r_w approaches zero. Hence, the steady state response is bounded when $r_f = 1.25$ and r_w approaches zero. It deserves to note that for the above case there is a two-root point at $r_w = 0.2$ as shown by a vertical dashed line shown in Fig. 9(b). Between three- and two-root points there is a small window for periodic without intermediate unloading motion.

Similarly, by Eq. (53) we can solve all admissible y in the range $(0, \pi]$. The results are displayed in Fig. 10 with $r_f = 2$ and 1.25. The smallest y curve is smooth for $r_f = 2$ and approaches zero when r_w approaches zero. However, the smallest y curve is non-smooth for $r_f = 1.25$, and it tends to a non-zero y when r_w approaches to zero. For this case the above two-root point disappears, and the periodic without intermediate unloading window between the 2 three-root points is enlarged.

In order to explain the jump phenomena as observed and indicated in Fig. 9(b), we return to Eq. (68) and rearrange it as

$$F(y, r_w, r_f) := (\tilde{c}\tilde{e} - \tilde{b}\tilde{f})^2 + (\tilde{a}\tilde{f} - \tilde{b}\tilde{c})^2 - r_f^2[\tilde{a}\tilde{e} - \tilde{b}^2]^2 + y = y. \tag{75}$$

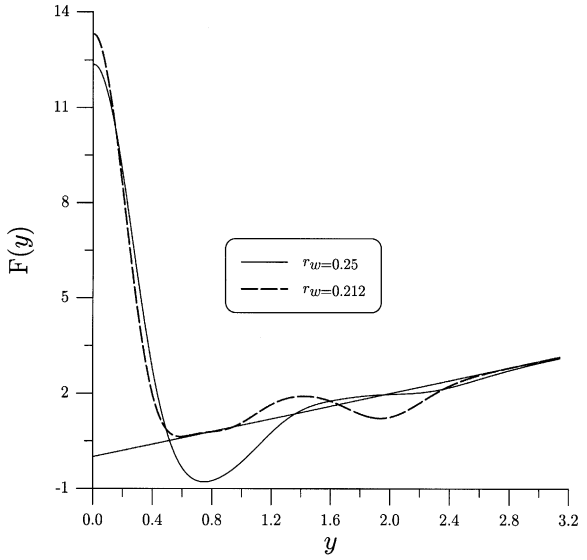

Fig. 11. Fixed $r_f = 1.25$ the curves of F used to find fixed points are plotted with $r_w = 0.25, 0.212$. The straight line is the bisection line.

For given r_f and r_w, when F maps a y to the same y there exists a fixed point for the map F and also a root for Eq. (68). At the fixed point y if $|dF/dy| > 1$ the fixed point is unstable, otherwise the fixed point is neutral stable or stable. Fixed $r_f = 1.25$ we plot two curves of F with respect to y in Fig. 11 by fixing $r_w(= 0.25$ and $0.212)$. It can be seen that at the first fixed (intersection) point of the $r_w = 0.25$ curve with the bisection line the slope $dF/dy > -1$ is negative, but for the $r_w = 0.212$ curve the slope $dF/dy > 1$ is just over unity and is unstable. This may explain why the steady state response jumps from a lower unstable value y to a higher stable value y. The above technique may be somewhat similar to the methods proposed by Miller and Butler [6] and Capecchi [8] in the instability analysis of their one-dimensional iterated maps. However, the above cited literature gave no explicit form of their iterated maps, but we give an exact form of the map F as shown in Eq. (75). It deserves to note that our method is more direct and effective than that proposed by Miller and Butler [6] and Capecchi [8].

Similarly, in order to explain the jumps appearing in Fig. 10(b) for the damped case to detect the stability/instability of the fixed points, we can employ the following map obtained from Eq. (53):

$$F(y, r_w, r_f, \zeta) := (\hat{c}\bar{e} - \bar{b}\hat{f})^2 + (\bar{a}\hat{f} - \hat{c}\bar{d})^2 - r_f^2[\bar{a}\bar{e} - \bar{b}\bar{d}]^2 + y = y. \tag{76}$$

Finally, according to the study of 10,000 $(= 100 \times 100)$ cases, we found that there were many types of steady state behaviour. In Fig. 12 the distribution of these types of behaviour is plotted in the plane $(r_w, 1/r_f)$ for two cases $\zeta = 0$ and $\zeta = 0.02$. When $r_w > 1/3$ no matter what r_f is there is only one root of y and hence the steady state motion is periodic without intermediate unloading, which is marked by circle in Fig. 12. For the undamped case there are also regions with multiple roots of y as shown in Fig. 12(a), which can be seen locating next to the points with inverse frequency ratio $1/r_w$ equal to odd integers; we only show the parametric points which lead to three

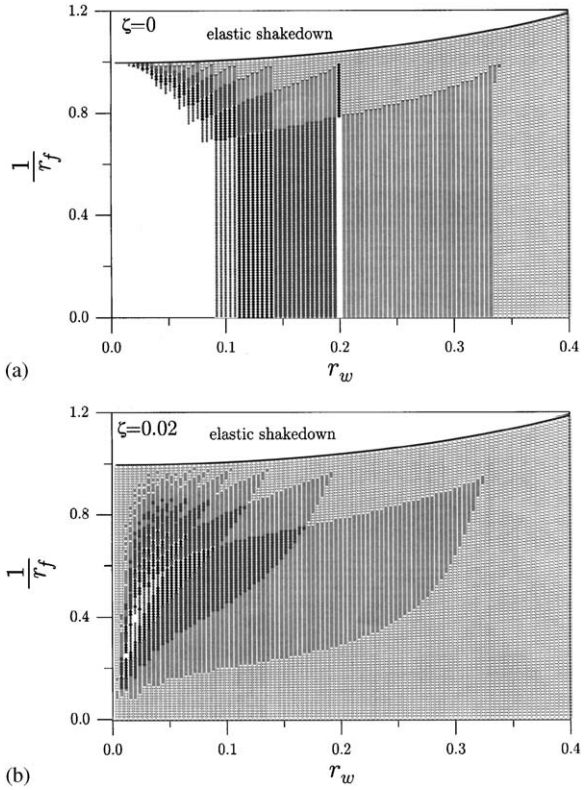

Fig. 12. In the parametric plane $(r_w, 1/r_f)$ below elastic shakedown curve the hysteretic response region, according to the number of the roots of y, is further classified into periodic without intermediate unloading and periodic with intermediate unloading regions for (a) $\zeta = 0$ and (b) $\zeta = 0.02$: ◦, one-root (periodic without intermediate unloading); ♦, two-root; ▩, three-root; ●, five-root; ▲, seven-root; ★, nine-root; blank, more roots. For the damped case there has no two-root point.

roots of y marked by solid square black points, five roots by solid black points, seven roots by solid triangular black points, nine roots by black star points, and more roots occupy the blank part. Especially, on the line $r_w = 0.2$ there are few points giving two roots of y as marked by solid lozenge black points.

In Fig. 3 we have displayed the responses with $r_w = 0.2$ and $r_f = 1.25$ among these points. The intermediate unloading occurs for this case; however, its time duration is rather short. This explains why our estimation is also good for this case as shown in Fig. 13. The distribution of the root numbers of y are shown in Fig. 12(b) for the damped case with $\zeta = 0.02$. It can be seen that the number of periodic points without intermediate unloading increases, the number of blank points reduces to only five, and the number of two-root points is zero. The multiple-root regions located next to the points with $\sqrt{1-\zeta^2}/r_w$ equal to odd integers. The damping term not only distorts the shapes of intermediate unloading motion region, but also moves the intermediate unloading motion region to the left. This region locates within the range of $r_w \leqslant \sqrt{1-\zeta^2}/3$, i.e., $\omega_d/\omega \leqslant 1/3$. Hence, the size of periodic without intermediate unloading region increases when damping ratio increases.

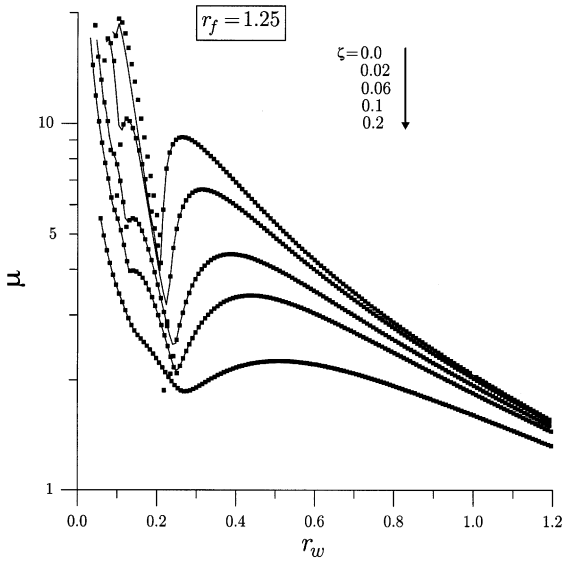

Fig. 13. The comparison of the frequency response curves with $r_f = 1.25$ which predicted respectively by ——, exact time-marching solutions, and ▩, phase-plane estimation method.

4. Concluding remarks

Through step-by-step time-marching calculations we have plotted the ductility ratio curves with respect to r_f and r_w for different damping ratios. The long-term behaviour has been classified into three types: elastic shakedown (including purely elastic), periodic with or without intermediate unloading in the parametric plane $(r_w, 1/r_f)$ for different ζ's. Closed-form formulae for estimating the steady state response in terms of the identified parameters y, r_f, r_w, and ζ were developed. The steady state solution presented in this paper is essentially exact inasmuch as the only approximation involved is in finding the root y of Eq. (53), which together with Eq. (58) provided a handy tool to study the long-term behaviour of viscous elasto-plastic oscillator. The validity and accuracy of the proposed formulae were confirmed, because the comparison of the results calculated from them with the exact time-marching solutions shows that they were in very good agreement with the exact ones no matter what frequency ratio range and force ratio are. In the low frequency ratio range the frequency response curves exhibit several subpeaks with steep variations, which intimately associate with the jump discontinuities of the smallest root of y in the intermediate unloading motion region. The intermediate unloading region can be identified with the appearance of multiple root of y at the parametric point in that region. For undamped case the subpeak which occurs at the point $r_w = 0.2$ has large depth valley; however, increasing the damping ratio renders the subpeak point move slightly to larger r_w and the depth of the valley is also decreased. We have shown the distribution of periodic points with or without intermediate unloading in the parametric plane $(r_w, 1/r_f)$, of which the intermediate unloading region locates within the range of $r_w \leqslant \sqrt{1-\zeta^2}/3$, i.e., $\omega_d/\omega \leqslant 1/3$, and its size decreases when damping ratio increases. The numerical tool provided here is more direct and more efficient than that proposed by Miller and Butler [6] and by Capecchi [8].

Appendix

In this appendix we provide exact solutions of Eqs. (12) and (14) under the loading (15).

1. *Elastic motion*:

$$x(t) = \exp[-\zeta\omega_n(t-t_i)][C_1\cos\omega(t-t_i) + C_2\sin\omega(t-t_i)] + A_1\sin\omega_d t - B_1\cos\omega_d t - \frac{r(t_i)}{k} + x(t_i), \tag{A.1}$$

where

$$\omega_n := \sqrt{\frac{k}{m}}, \quad \zeta := \frac{c}{2m\omega_n}, \quad \omega := \omega_n\sqrt{1-\zeta^2} \tag{A.2–A.4}$$

are, respectively, the natural frequency, damping ratio and damped frequency of the structure. Here and henceforth we assume $\zeta < 1$, such that the system is underdamped in the elastic phase. A_1 and B_1 are defined, respectively, by

$$A_1 := \frac{r_f x_y(1-r_w^2)}{(1-r_w^2)^2 + 4\zeta^2 r_w^2}, \tag{A.5}$$

$$B_1 := \frac{2r_f x_y \zeta r_w}{(1-r_w^2)^2 + 4\zeta^2 r_w^2}, \tag{A.6}$$

where

$$r_f := \frac{p_0}{r_y}, \quad r_w := \frac{\omega_d}{\omega_n}, \quad x_y := \frac{r_y}{k} \tag{A.7–A.9}$$

are, respectively, the force ratio, frequency ratio and yield displacement. The two integration constants C_1 and C_2 are given, respectively, by

$$C_1 := B_1\cos\omega_d t_i - A_1\sin\omega_d t_i + \frac{r(t_i)}{k}, \tag{A.10}$$

$$C_2 := \frac{\dot{x}(t_i)}{\omega} + \frac{[B_1\zeta - A_1 r_w]\cos\omega_d t_i}{\sqrt{1-\zeta^2}} - \frac{[B_1 r_w + A_1\zeta]\sin\omega_d t_i}{\sqrt{1-\zeta^2}} + \frac{\zeta r(t_i)}{k\sqrt{1-\zeta^2}}. \tag{A.11}$$

The constitutive force r appeared in the above should be supplemented with Eq. (13) during elastic motion interval.

2. *Plastic motion*:

$$x(t) = C_4 + C_3\exp[-2\zeta\omega_n(t-t_i)] - A_2\sin\omega_d t - B_2\cos\omega_d t - \frac{r(t_i)}{c}t, \tag{A.12}$$

where

$$A_2 := \frac{r_f x_y}{r_w^2 + 4\zeta^2}, \tag{A.13}$$

$$B_2 := \frac{2r_f x_y \zeta}{r_w(r_w^2 + 4\zeta^2)}, \tag{A.14}$$

and the two integration constants C_3 and C_4 are given, respectively, by

$$C_3 \coloneqq A_2 \sin \omega_d t_i - \frac{r_w}{2\zeta} A_2 \cos \omega_d t_i - \frac{\dot{x}(t_i)}{2\zeta\omega_n} - \frac{r(t_i)}{2\zeta\omega_n c}, \tag{A.15}$$

$$C_4 \coloneqq \left[B_2 + \frac{r_w}{2\zeta} A_2\right] \cos \omega_d t_i + \frac{r(t_i)}{2\zeta\omega_n c} + \frac{t_i r(t_i)}{c} + x(t_i) + \frac{\dot{x}(t_i)}{2\zeta\omega_n}. \tag{A.16}$$

The constitutive force is simply $r(t) = r(t_i)$ during plastic motion interval. Unlike in the elastic motion, whose response when $r_w = 1$ has a peak value due to resonance, in the plastic motion as shown in Eq. (A.12) there never occurs plastic resonance.

The transition points between elastic and plastic motions are determined by the on–off switch criteria (9) and (10).

3. *Determination of the onset of plastic motion*: Given the initial values $r(t_i)$ and $\dot{x}(t_i)$ at an initial time t_i, the transition time from elastic motion to plastic motion can be determined by solving the equation $|r(t)| = r_y$, where $r(t)$ is obtained by substituting Eq. (A.1) into Eq. (13). The resulting equation is transcendental in nature so that a numerical method may be invoked to calculate the switch-on time $t = t_{on}$.

4. *Transition from plastic motion to elastic motion*: When a plastic motion interval is switched off at a time moment, i.e., $|r| < r_y$ or $r\dot{x} \leqslant 0$, the structure will switch to an elastic motion with certain time interval according to the switching criterion (10). The end time of the plastic motion is determined by solving $\dot{x}(t) = 0$ for t, which is also a transcendental equation still requiring a numerical method to calculate the switch-off time $t = t_{off}$.

Determination of the transition times t_{on} and t_{off} can easily be carried out to arbitrary accuracy. However, due to the periodicity and transcendentality of the considered equations we prefer to solve them by using half-interval method rather than the usual Newton–Raphson method. In practical calculations the error tolerance is controlled within the order of 10^{-10}.

By piecing the above two solutions (A.1) and (A.12) of elastic and plastic motions together and with accurately determined t_{on} and t_{off}, the essentially exact responses of the viscous elasto-plastic oscillator can be obtained. The dynamics of the model may switch between the two motions.

References

[1] T.K. Caughey, Sinusoidal excitation of a system with bilinear hysteresis, *Journal of Applied Mechanics, American Society of Mechanical Engineers* 32 (1960) 640–648.

[2] S.F. Masri, Forced vibration of the damped bilinear hysteretic oscillator, *Journal of the Acoustical Society of America* 57 (1975) 106–112.

[3] R. Pratap, S. Mukherjee, F.C. Moon, Dynamic behavior of a bilinear hysteretic elasto-plastic oscillator. Part I: free oscillations, Part II: oscillations under periodic impulse forcing, *Journal of Sound and Vibration* 172 (1994) 321–358.

[4] C.-S. Liu, Exact solutions and dynamic responses of SDOF bilinear elastoplastic structures, *Journal of the Chinese Institute of Engineers* 20 (1997) 511–525.

[5] M.A. Savi, P.M.C.L. Pacheco, Non-linear dynamics of an elasto-plastic oscillator with kinematic and isotropic hardening, *Journal of Sound and Vibration* 207 (1997) 207–226.

[6] G.R. Miller, M.E. Butler, Periodic response of elastic-perfectly plastic SDOF oscillator, *Journal of Engineering Mechanics, American Society of Civil Engineers* 114 (1988) 536–550.

[7] D. Capecchi, Periodic response and stability of hysteretic oscillator, *Dynamics and Stability of Systems* 6 (1991) 89–106.
[8] D. Capecchi, Asymptotic motions and stability of the elastoplastic oscillator studied via maps, *International Journal of Solids and Structures* 23 (1993) 3303–3314.
[9] C.-S. Liu, The steady loops of SDOF perfectly elastoplastic structures under sinusoidal loadings, *Journal of Marine Science and Technology* 8 (2000) 50–60.
[10] Z.-M. Huang, The Vibration Behavior of Single-Degree-of-Freedom Smoothing and Bilinear Viscous-Elastoplastic Oscillators under Sinusoidal Loadings, Master Thesis, Department of Mechanical and Marine Engineering, National Taiwan Ocean University, Keelung, Taiwan, 2002.
[11] D. Capecchi, F. Vestroni, Steady-state dynamic analysis of hysteretic systems, *Journal of Engineering Mechanics, American Society of Civil Engineers* 111 (1985) 1515–1531.
[12] D. Capecchi, F. Vestroni, Periodic response of a class of hysteretic oscillators, *International Journal of Non-Linear Mechanics* 25 (1990) 309–317.
[13] A. DebChaudhury, Periodic response of yielding oscillators, *Journal of Engineering Mechanics, American Society of Civil Engineers* 111 (1985) 977–994.
[14] F. Badrakhan, Dynamic analysis of yielding and hysteretic systems by polynomial approximation, *Journal of Sound and Vibration* 125 (1988) 23–42.
[15] R. Pratap, P. Holmes, Chaos in a mapping describing elastoplastic oscillations, *Nonlinear Dynamics* 8 (1995) 111–139.
[16] C.K. Reddy, R. Pratap, Equivalent viscous damping for a bilinear hysteretic oscillator, *Journal of Engineering Mechanics, American Society of Civil Engineers* 126 (2000) 1189–1196.
[17] H.-K. Hong, C.-S. Liu, Prandtl–Reuss elastoplasticity: on-off switch and superposition formulae, *International Journal of Solids and Structures* 34 (1997) 4281–4304.